Bulletin of the Seismological Society of America, 89, 3, pp. 733–741, June 1999

A Simple Orthonormalization Method for Stable and Efficient Computation of Green's Functions

by Rongjiang Wang

Abstract Some major matrix methods for computation of Green's functions of a layered half-space model are compared. It is known that the original Thomson–Haskell propagator algorithm has the loss-of-precision problem when waves become evanescent. The minor matrix extension solves to some extent the numerical problem but at the expense of the computational efficiency. At present, the recursive technique (the reflectivity method) is used by most seismologists. An alternative algorithm is presented that uses the same strategy as the original propagator algorithm but avoids the numerical problem by inserting an additional numerical procedure into the matrix propagation loop. The new technique is simple and efficient, and in particular, it is not only applicable to the matrix method but also to any numerical integration method for general use. High-frequency synthetic seismograms are computed for modeling significant site effects such as observed in the aftershocks of the Latur earthquake, 1993, India.

Introduction

In modeling of geophysical processes, the media are often approximated by a stratified half-space. The reason is that on one hand, the approximation satisfies the required modeling accuracy in a wide range of applications, and on the other hand, the Green's functions of such media supply useful references for results of more complicated models. Since the early fifties, numerical methods for such models have improved continuously. Developments were aimed mostly at numerical stability and computational efficiency.

Thomson (1950) and Haskell (1953) may be the first who introduced the propagator algorithm into computational seismology. The terminology of propagator stems from calculating the displacement vector (in the frequency-wavenumber domain) from layer to layer via a chain rule. The Thomson–Haskell propagator algorithm is simple to use. However, as was found quite early, its results exhibit numerical instabilities when waves become evanescent. The difficulty can be avoided to some extent by working directly in terms of minors of the propagator matrix (Knopoff, 1964; Dunkin, 1965). The disadvantage of such an extension is that it requires an artificial upper limit of the layer thickness (Kind, 1983; Schwab *et al.*, 1984) and results therefore in higher computation expense. Presently, the recursive algorithm given by Kennett (1983) is widely used that was developed on the basis of many earlier works (e.g., Fuchs, 1968; Fuchs and Müller, 1971; Kenneth and Kerry, 1979). Because it works with the reflection-transmission coefficient matrix, the recursive algorithm is called simply the "reflectivity method" by many seismologists. Chin *et al.* (1984) have shown that the recursive algorithm is actually an invariant embedding that is known to be equivalent to Gaussian elimination. The latter explains the stability of the method in the evanescent case. A global matrix approach is given by Chin *et al.* (1984) and Schmidt and Tango (1986) for more computational efficiency.

The numerical stability is not only important for synthetic seismograms but also for computations of static deformations based on the elastic dislocation theory. Jovanovich *et al.* (1974) proposed a quasi-analytical extension in which the Thomson–Haskell propagator matrix of each layer is decomposed into the sum of four matrices weighted with different exponentials. The aim is to avoid numerical operations between extreme large and small exponentials that cause the loss-of-precision problem. No doubt, the quasi-analytical formulation is stable, but the required storage increases exponentially with the number of the layers. For personal computers at present, only few-layered (max. 5 to 6) models can be computed in practice (Roth, 1997, personal comm.). Another way is to generalize the reflectivity method for the static displacement field (e.g., Xie and Yao, 1989).

Similar numerical problems have also been reported in modeling postglacial rebound. Wu and Peltier (1982) and Han and Wahr (1995) found, for instance, significant numerical noise that affects the finding of the long-term viscogravitational relaxation modes. Although they solved the equations of motion by the Runge–Kutta integration instead of the matrix method, the cause for the numerical difficulty should be the same. As we know presently, the problem in this field remains still unsolved.

In this article, we present an alternative propagator algorithm with a global solution strategy. By using the Thomson–Haskell propagator rule, we determine in parallel all independent displacement vectors from the surface downward and from infinity upward as well to the source plane. These vectors are the fundamental solutions for different source mechanisms. The desired solution is finally superposed by using the given source conditions. As the vectors at all layer interfaces are stored, the depth-dependent Green's functions are then determined by only one pass.

The remaining problem is how to avoid the numerical difficulty. First, we look into the physics of the problem. In the evanescent case, the most rapidly growing wave becomes dominant in all fundamental displacement vectors and reduces consequently their independence from each other. Fortunately, there is a certain freedom of choice of the fundamental vectors. In fact, they construct a complete system of vector bases of the solution space. As for a coordinate system, the vector bases can be scaled and oriented arbitrarily. This property allows us to insert an additional procedure into the propagation loop that makes all fundamental vectors in situ orthonormal; that means, before each layer to be passed, the vectors are brought into correspondence with each other and reconstructed so that they are of the same order (normal) and include the different main waves separately (orthogonal). So, there will be no numerical operations between different growing functions and no loss-of-precision problem, independent of the thickness of the layers.

It should be pointed out that the idea using correspondence among the basic solution vectors for stabilizing Green's function computations has been used for a long time. Takeuchi and Saito (1972), for example, introduced a set of new variables in terms of the two independent *P-SV* solutions for stabilizing the Rayleigh-wave computation using the numerical integration of the differential equations and have shown its equivalence to the minor matrix formulations by Dunkin (1965) and Gilbert and Backus (1966). The specific advantage of the present orthonormalization approach is that it applies only a minor extension to the simplest Haskell propagator scheme, and the variables to be propagated remain the displacement vectors that are what we need directly. The latter feature guarantees more efficiency in comparison to various previous algorithms, particularly for computation of depth-dependent Green's functions, as the vector propagation through the layers is computed once for all.

In the two application examples, we have applied the new algorithm to the computations of static deformations and synthetic seismograms. The results of the latter example are used for modeling the local resonance effects as such observed in the aftershocks of the Latur earthquake, 1993, India (Baumbach *et al.*, 1994).

The Basic Theory

We consider a Green's function problem for a stack of homogeneous layers above a homogeneous half-space and use the cylindrical coordinate system $\mathbf{x} = (r, \theta, z)$ with z to be directed downward. The vertical stratification of the model is shown in Table 1 where the parameters ρ, λ, and μ are the density and the two Lamé constants, respectively. A point source is assumed to be situated at $\mathbf{x}_s = (0, 0, z_s)$. As shown later, it is convenient to define the source plane as a pseudo-layer interface.

In general, we can use the Fourier–Hankel transform to convert any linearized equations of motion to a system of ordinary differential equations. In a region without the source, the equation system is written in the following matrix form:

$$\frac{d}{dz}\mathbf{y} = \mathbf{A}\mathbf{y}, \tag{1}$$

where $\mathbf{y}$ is the generalized displacement vector representing a set of physical observables in the frequency-wavenumber domain, and $\mathbf{A}$ is the coefficient matrix depending on the parameters of the medium. The desired solution for $\mathbf{y}$ should satisfy the boundary conditions given at both ends of the model, that is, at $z = 0$ and $z \to \infty$, and the continuity conditions at all interfaces in the interior, $z = z_i\ (i = 2, \ldots, n)$. In words of the mathematical-physical terminology, this is a two-point boundary value problem. The influence of the point source can be expressed by a discontinuity of the solution vector $\mathbf{y}$ across the source plane $z = z_s$:

$$[\mathbf{y}]_-^+ = \mathbf{y}(z_s^+) - \mathbf{y}(z_s^-) = \Delta\mathbf{y}_s, \tag{2}$$

where z_s^- and z_s^+ are the upper and lower side of the source plane, respectively, and $\Delta\mathbf{y}_s$ is the Hankel-transformed source function [for seismological applications, see, e.g., Kennett and Kerry (1979) or Kennett (1983)].

As is known, it is more complicated to solve a two-point boundary value problem than an initial value problem. In the latter case, we can integrate equation (1) with a starting value given at the one end and obtain the solution step by step until we arrive at the other end. In the present case, neither the boundary conditions at the surface nor those at infinity can determine a unique solution there. In the next section, we propose a global solution approach in which equation (1) is integrated from both ends to the source plane with independent starting values to determine all fundamental solutions satisfying different source mechanisms. The desired

Table 1
Coding of a Stratified Half-Space Model

Layer	Parameters	Upper z	Lower z	Thickness
1	$\rho_1, \lambda_1, \mu_1, \ldots$	$z_1 = 0$	z_2	h_1
...	...	...	...	...
i	$\rho_i, \lambda_i, \mu_i, \ldots$	z_i	z_{i+1}	h_i
...	...	...	...	...
n	$\rho_n, \lambda_n, \mu_n, \ldots$	z_n	∞	∞

solution is then obtained by a superposition of the fundamental solutions so that the given source condition (equation 2) is satisfied. The procedure becomes of course easier when all fundamental solutions can be given in analytical form. In computational seismology, all parameters in each layer are therefore commonly approximated by a constant value. In this case, all fundamental solutions are given by exponential functions, and the Green's function problem is finally converted to a matrix problem.

A Global Solution Approach with the Propagator Algorithm

In most geophysical applications, the vector $\mathbf{y}$ in equation (1) has $2N$ ($N = 1,2, \ldots$) components. Without loss of generality, we consider a seismic Green's function in the *P-SV* case with $N = 2$ and define

$$\mathbf{y} = (U, V, P, S)^T, \tag{3}$$

where U and V are the two displacement components in the frequency-wavenumber domain and P and S are the two components of the elastic surface force on a horizontal plane. For a homogeneous layer, the analytical solutions of $\mathbf{y}$ have been found and can be written in the form

$$\mathbf{y} = \mathbf{LEc}, \tag{4}$$

where $\mathbf{L}$ is a 4×4 layer matrix consisting of the eigenvectors of the coefficient matrix $\mathbf{A}$ of equation (1) [for its entries in detail, see, e.g., Aki and Richards (1980) or Kennett (1983)], $\mathbf{E}$ is a 4×4 diagonal matrix,

$$\mathbf{E} = \begin{pmatrix} e^{\alpha z} & 0 & 0 & 0 \\ 0 & e^{\beta z} & 0 & 0 \\ 0 & 0 & e^{-\alpha z} & 0 \\ 0 & 0 & 0 & e^{-\beta z} \end{pmatrix}, \tag{5}$$

and $\mathbf{c}$ is a four-dimensional constant vector to be determined,

$$\mathbf{c} = (A_+, B_+, A_-, B_-)^T. \tag{6}$$

The parameters $\pm\alpha$ and $\pm\beta$ in equation (5) are the eigenvalues of $\mathbf{A}$ and represent in the case treated here the vertical wavenumbers of the P and SV waves,

$$\left.\begin{aligned} \alpha &= \sqrt{k^2 - \frac{\omega^2}{V_p^2}}, \\ \beta &= \sqrt{k^2 - \frac{\omega^2}{V_s^2}}, \end{aligned}\right\} \tag{7}$$

where $V_p = \sqrt{(\lambda + 2\mu)/\rho}$ and $V_s = \sqrt{\mu/\rho}$ are the two isotropic seismic velocities, ω is the frequency, and k is the horizontal wavenumber (the Hankel variable). The notations with $A_\pm$ and $B_\pm$ for the constants in equation (6) are used for indicating whether the waves are going upward or downward.

As can be seen, for $\omega \to 0$, both $\alpha, \beta \to k$. In this case, the four fundamental wave solutions $e^{\pm\alpha z}$ and $e^{\pm\beta z}$ should be replaced by the static solutions, $e^{\pm kz}$ and $ze^{\pm kz}$, and the layer matrix should be modified correspondingly.

If the displacement vector $\mathbf{y}$ is given at the ith interface, $z = z_i$, its value at the next interface, $z = z_{i+1}$, can be obtained via a simple propagation rule:

$$\mathbf{y}_{i+1} = \mathbf{H}_i \mathbf{y}_i, \tag{8}$$

where $\mathbf{H}_i$ is the 4×4 Thomson–Haskell propagator matrix depending on the parameters of the ith layer:

$$\mathbf{H}_i = \mathbf{L}_i\mathbf{E}_i(z_{i+1})\mathbf{E}_i^{-1}(z_i)\mathbf{L}_i^{-1} = \mathbf{L}_i\mathbf{E}_i(h_i)\mathbf{L}_i^{-1}, \tag{9}$$

with $h_i = z_{i+1} - z_i$ being the layer thickness. The inverse forms of equations (8) and (9) are simply

$$\mathbf{y}_i = \mathbf{H}_i^{-1}\mathbf{y}_{i+1}, \tag{10}$$

and

$$\mathbf{H}_i^{-1} = \mathbf{L}_i\mathbf{E}_i(-h_i)\mathbf{L}_i^{-1}. \tag{11}$$

Note that at the free surface $z = z_1 = 0$, the displacement vector has the form

$$\mathbf{y}_1 = (U, V, 0, 0)^T, \tag{12}$$

and at the lowest interface $z = z_n$,

$$\mathbf{y}_n = \mathbf{L}_n(0, 0, A_-, B_-)^T, \tag{13}$$

because there are no upgoing waves from infinity.

It is obvious that neither $\mathbf{y}_1$ nor $\mathbf{y}_n$ can be used as the starting value of the vector propagation because they include just the parameters that are unknown. The strategy of our global solution approach consists of the following three steps.

1. Define two vector bases at the surface, which can be orthonormal, but need not be so, for example,

$$\hat{\mathbf{Y}}_1 = (\hat{\mathbf{y}}_1^{(1)}, \hat{\mathbf{y}}_1^{(2)}) = \begin{pmatrix} 1 & 0 \\ 0 & 1 \\ 0 & 0 \\ 0 & 0 \end{pmatrix}, \tag{14}$$

and decompose the surface displacement vector as

$$\mathbf{y}_1 = U\hat{\mathbf{y}}_1^{(1)} + V\hat{\mathbf{y}}_1^{(2)}. \tag{15}$$

Similarly, we define the vector bases at $z = z_n$,

$$\hat{\mathbf{Y}}_n = (\hat{\mathbf{y}}_n^{(1)}, \hat{\mathbf{y}}_n^{(2)}) = \mathbf{L}_n \hat{\mathbf{C}}_n, \tag{16}$$

where

$$\hat{\mathbf{C}}_n = (\hat{\mathbf{c}}_n^{(1)}, \hat{\mathbf{c}}_n^{(2)},) = \begin{pmatrix} 0 & 0 \\ 0 & 0 \\ 1 & 0 \\ 0 & 1 \end{pmatrix}, \tag{17}$$

and decompose the displacement vector there by

$$\mathbf{y}_n = A\_\hat{\mathbf{y}}_n^{(1)} + B\_\hat{\mathbf{y}}_n^{(2)}. \tag{18}$$

2. Determine the global vector bases $\hat{\mathbf{Y}}_i$, for $z = z_1, \ldots, z_i, \ldots, z_s^-$, and $\hat{\mathbf{Y}}_j$, for $z = z_n, \ldots, z_j, \ldots, z_s^+$, via the propagator algorithm with $\hat{\mathbf{Y}}_1$ and $\hat{\mathbf{Y}}_n$ as the starting values at $z = z_1 = 0$ and at $z = z_n$, respectively.
3. Find the decomposition constants by the source condition,

$$A\_\hat{\mathbf{y}}_s^{(1)}(z_s^+) + B\_\hat{\mathbf{y}}_s^{(2)}(z_s^+) = U\hat{\mathbf{y}}_s^{(1)}(z_s^-) + V\hat{\mathbf{y}}_s^{(2)}(z_s^-) + \Delta\mathbf{y}_s, \tag{19}$$

and give finally the global displacement vector,

$$\mathbf{y}_i = \begin{cases} U\hat{\mathbf{y}}_i^{(1)} + V\hat{\mathbf{y}}_i^{(2)} & \text{for } i = 1, \ldots, s-1, \\ A\_\hat{\mathbf{y}}_j^{(1)} + B\_\hat{\mathbf{y}}_j^{(2)}, & \text{for } j = s+1, \ldots, n. \end{cases} \tag{20}$$

An obvious advantage of the present global approach is that it avoids a large system of matrix equations. The depth-dependent vector bases are calculated by one pass and need only to be stored for depths where the solution is really desired. The other important advantage is that it supplies a convenient formulation for solving the numerical problem. The latter will be seen in the next section.

A Simple Method to Avoid Numerical Instabilities

The physical cause of the numerical difficulty of the propagator algorithm becomes quite clear with the present global approach. In the evanescent case, that is, when the real part of the wavenumber α or β does not vanish, the wave with the most rapidly increasing exponential is going to be dominant over all others after a thick layer has been passed. As a consequence, the two vector bases lose more and more of their independence from each other. With the always limited computation accuracy, they become in the extreme even parallel when the propagation arrives at the source plane and the determinant of the coefficient matrix of equation (19) vanishes.

It should be emphasized that the problem is not caused by operations between the increasing and decreasing exponentials, as it may be supposed at first sight, but by operations between the two different increasing exponentials. This

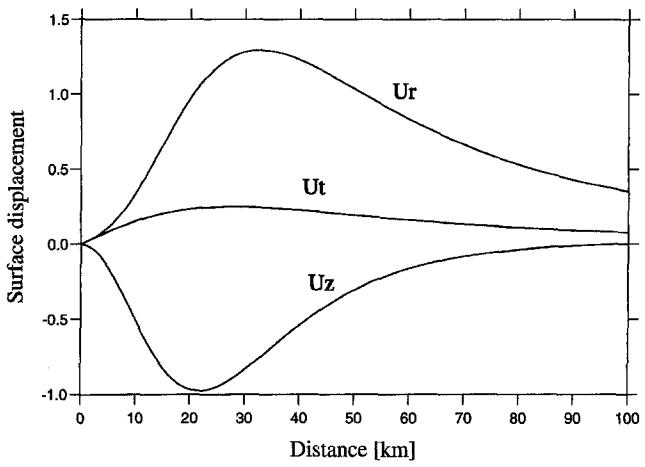

Figure 1. Arbitrarily normalized static surface displacements calculated for the seismic model IASP91 (Kennett and Engdahl, 1991). A strike-slip point source is situated at depth of 30 km. The vertical (downward positive), radial, and tangential components are denoted by *Uz*, *Ur*, and *Ut*, respectively. The azimuth dependence is given by the factor sin 2θ for the vertical and radial components and cos 2θ for the tangential component where θ is the azimuth angle relative to the strike.

can be understood easily from the physical point of view. The increasing exponentials represent the incident waves from the source, while the decreasing exponentials are their reflections from an interface. If the interface is far enough from the source, the reflected waves cannot be detected when they are all evanescent. Therefore, it is natural that the terms of decreasing exponentials may vanish numerically after a thick layer has been passed. Both incident waves, however, are growing waves while approaching the source and include complementary informations about the response of the medium. If one of them loses little by little its presence due to the limited computation accuracy, the source conditions are not matched correctly, and the results become consequently unstable. In this way, we explain also why a toroidal (*SH*) system of second order is always stable because there is only one incident wave.

Our idea for solving the difficulty is to reconstruct the vector bases depth to depth so that their independence can be protected in situ. Because the vector bases can be scaled and oriented arbitrarily as with a coordinate system, we are allowed to insert an additional procedure into the propagation loop that makes the vector bases orthonormal so that they include the two growing waves separately. In the following, we give a flowchart in a program-ready form to demonstrate the propagation rule from the surface to the source plane.

1. Start the vector propagation with $\hat{\mathbf{Y}}_i = \hat{\mathbf{Y}}_1$.
2. Determine the corresponding constant vector bases $\hat{\mathbf{C}}_i$ for the ith layer by

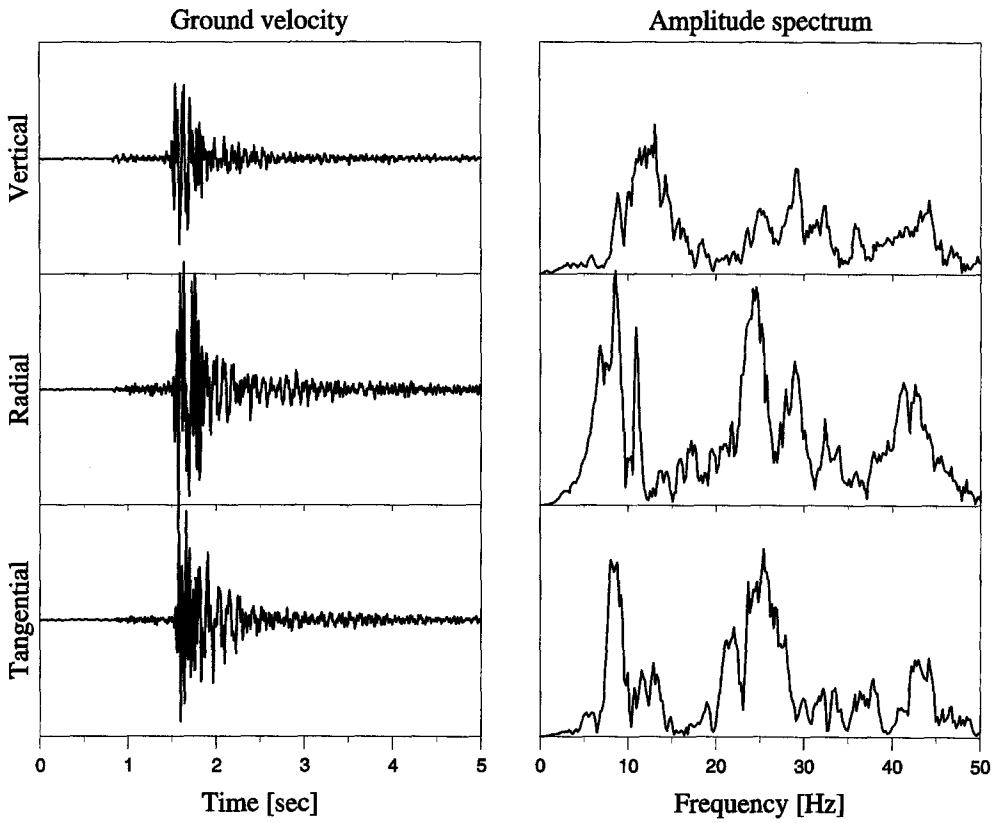

Figure 2. An example of typical aftershock seismograms observed in the Killari area. The epicentral distance is about 3 km.

$$\hat{\mathbf{C}}_i = \mathbf{L}_i^{-1}\,\hat{\mathbf{Y}}_i. \tag{21}$$

3. Normalize $\hat{\mathbf{Y}}_i$ and $\hat{\mathbf{C}}_i$ and, if necessary, all those in the storage,

$$\left.\begin{aligned}\hat{\mathbf{Y}}_j &:= \hat{\mathbf{Y}}_j\mathbf{N},\\ \hat{\mathbf{C}}_j &:= \hat{\mathbf{C}}_j\mathbf{N},\end{aligned}\right\} \quad \text{for } j = 1, \ldots, i, \tag{22}$$

with

$$\mathbf{N} = \begin{pmatrix} |\hat{\mathbf{c}}_i^{(1)}|^{-1} & 0 \\ 0 & |\hat{\mathbf{c}}_i^{(2)}|^{-1}\end{pmatrix}, \tag{23}$$

where denotes reset. This step is necessary to avoid overflow and operations between values of different orders in the next step.

4. Define a 2×2 manipulation matrix $\mathbf{Q}$

$$\mathbf{Q} = \begin{pmatrix} \hat{C}_{i,22} & -\hat{C}_{i,12} \\ -\hat{C}_{i,21} & \hat{C}_{i,11}\end{pmatrix}, \tag{24}$$

where $\hat{C}_{i,12}$ is the element of $\hat{\mathbf{C}}_i$ of row 1 and column 2, and so on, and reconstruct the vector bases by

$$\left.\begin{aligned}\hat{\mathbf{Y}}_j &:= \hat{\mathbf{Y}}_j\mathbf{Q},\\ \hat{\mathbf{C}}_j &:= \hat{\mathbf{C}}_j\mathbf{Q},\end{aligned}\right\} \quad \text{for } j = 1, \ldots, i. \tag{25}$$

Note that after reset, $\hat{C}_{i,12}(B_+) = 0$ and $\hat{C}_{i,21}(A_+) = 0$, that means, for the ith layer, the first vector includes the upgoing P wave and its corresponding reflections from the interface at the top; the second includes the upgoing SV wave and so on.

5. Make the vector propagation to the next interface,

$$\hat{\mathbf{Y}}_{i+1} = \mathbf{L}_i\mathbf{E}_i(h_i)\hat{\mathbf{C}}_i. \tag{26}$$

Because there are no more operations between the growing P and SV waves, the loss-of-precision problem is therefore fully avoided, no matter how thick the layer is.

To get more efficiency, steps 3 and 4 can be combined into one step. Then the manipulation matrix $\mathbf{Q}$ should be scaled by the normalization factor $|\hat{\mathbf{c}}_i^{(1)}| \cdot |\hat{\mathbf{c}}_i^{(2)}|$. Additionally, note that the required conditions $\hat{C}_{i,12}(B_+) = \hat{C}_{i,21}(A_+) = 0$ could not be satisfied exactly because of numerical round off. In practice, it is therefore necessary to explicitly set them to zero after the orthonormalization.

The propagation from the lowest interface upward to the source plane can be done similarly. The only difference

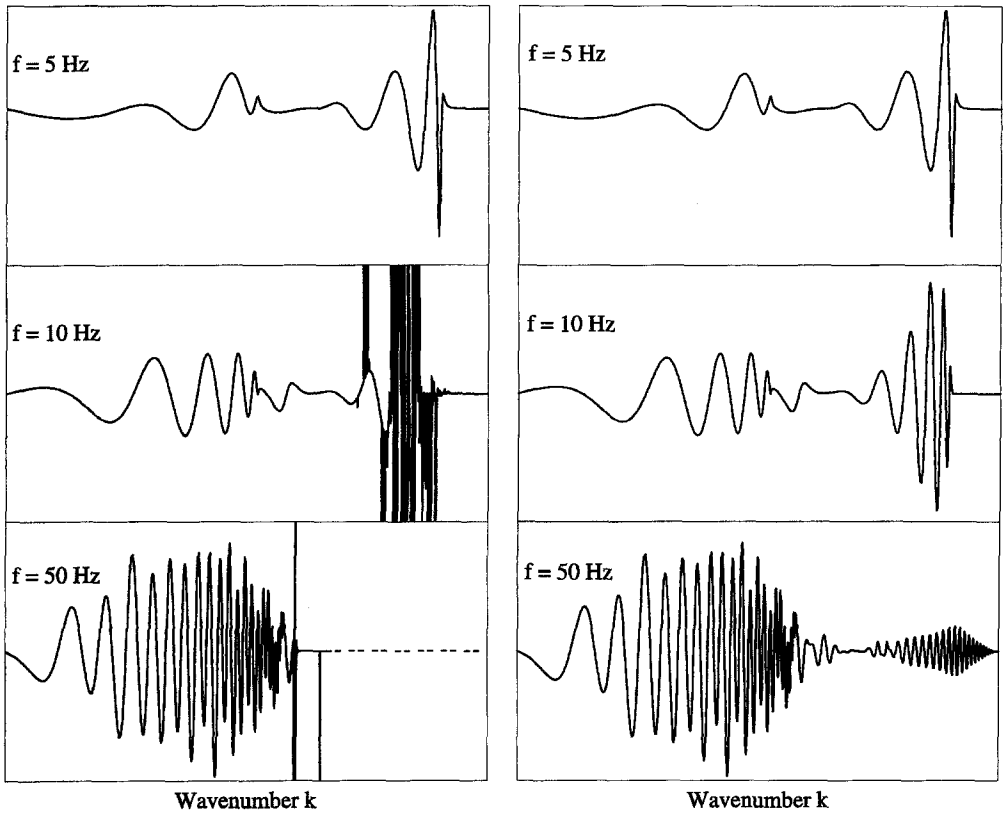

Figure 3. Arbitrary examples for numerical results of the original Thomson–Haskell propagator algorithm (*left*) and of the new propagator algorithm with the orthonormalization technique (*right*). The graphs represent the real part of the vertical displacement in the frequency-wavenumber domain calculated for the Killari model (Table 2) with a point source at depth of 3 km. Numerical difficulties of the original propagator method arise in the range of high frequencies and large wavenumbers. In the extreme, it does not even work anymore (dashed line), while the new algorithm remains stable overall (the frequency has been turned in the tests up to 1 kHz without causing any instabilities).

is that in step 4 the vector bases are made orthogonal with respect to the downgoing waves instead of the upgoing waves. In comparison to the algorithms used previously for numerical stabilities, the present orthonormalization technique has advantages for both physical insight and computational efficiency. Furthermore, it is possible as in the reflectivity method to isolate individual arrivals if we select one of the vector bases that is associated with a certain incident wave and set the others to zero.

In particular, with a small modification, the present technique can be used to extend the numerical integration for the general use. When the entries of the coefficient matrix **A** in equation (1) are functions of the depth, direct integration methods with the Runge–Kutta technique, for example, are often used, and the same numerical problem is expected. In this case, we propose to orthonormalize the vector bases step by step via the following rule:

$$\hat{\mathbf{y}}^{(i)} := \hat{\mathbf{y}}^{(i)}/|\hat{\mathbf{y}}^{(i)}|, \; i = 1,2, \ldots$$

$$\hat{\mathbf{y}}^{(1)} := \hat{\mathbf{y}}^{(1)};$$

$$\hat{\mathbf{y}}^{(2)} := \hat{\mathbf{y}}^{(2)} + a \cdot \hat{\mathbf{y}}^{(1)}, \qquad \text{so that } \hat{\mathbf{y}}^{(2)} \perp \hat{\mathbf{y}}^{(1)};$$

$$\hat{\mathbf{y}}^{(3)} := \hat{\mathbf{y}}^{(3)} + b \cdot \hat{\mathbf{y}}^{(1)} + c \cdot \hat{\mathbf{y}}^{(2)}, \qquad \text{so that } \hat{\mathbf{y}}^{(3)} \perp \hat{\mathbf{y}}^{(1)} \text{ and } \perp \hat{\mathbf{y}}^{(2)};$$

$$\cdots .$$

After some steps, the most rapidly growing wave will be dominant in $\hat{\mathbf{y}}^{(1)}$, and the others are separately in $\hat{\mathbf{y}}^{(2)}$, $\hat{\mathbf{y}}^{(3)}$, . . . , and so on. The loss-of-precision problem can therefore be solved as similarly as in the matrix method. In a forthcoming article, we will show that the numerical noise as such reported in Wu and Peltier (1982) and Han and Wahr (1995) can be removed with our method successfully.

Table 2
Model for the Killari Area (Baumbach *et al.*, 1994)

Layer	ρ (g/cm^3)	V_p (km/sec)	V_s (km/sec)	Q_p	Q_s	h (m)
1	1.3	1.2	0.2	80	20	5
2	2.5	4.5	2.6	500	220	300
3	2.7	6.0	3.5	800	270	∞

Application Examples

Static Deformations Due to a Dislocation Source

The elastic dislocation theory is a useful tool for modeling quasi-static co-seismic as well as post-seismic deformations. For the simplest homogeneous half-space model, analytical solutions given by Mindlin (1936) and Mindlin and Cheng (1950), or in a more extended form by Okada (1992), can be used. When a realistic layered model is computed by the propagator algorithm, however, there appear often numerical instabilities. The problem has been solved presently with the quasi-analytical algorithm given by Jovanovich *et al.* (1974), provided that the model has only a few layers. Xie and Yao (1989) generalized the reflectivity method to the static case by suitable definition of the reflection-transmission matrices. We have tested the orthonormalization method for models with a large number of layers. Figure 1 shows an example computed for the seismic model IASP91 (Kennett and Engdahl, 1991). A strike-slip point source is situated at a depth of 30 km. In the computation, the piecewise continuous stratification of the model has been approximated by more than 500 homogeneous layers. Even though different from the dynamic case, such fine resolution for a static model is not necessary, the purpose here was to demonstrate the power of the new algorithm.

Modeling of the Local Resonance Effects

In this example, we apply the new propagator algorithm to synthetic seismograms for modeling the significant site effects observed in a number of aftershocks of the Latur earthquake, 1993, India (Baumbach *et al.*, 1994). Such site effects are of much importance to the structural engineering. For buildings whose eigenfrequencies are placed in the local

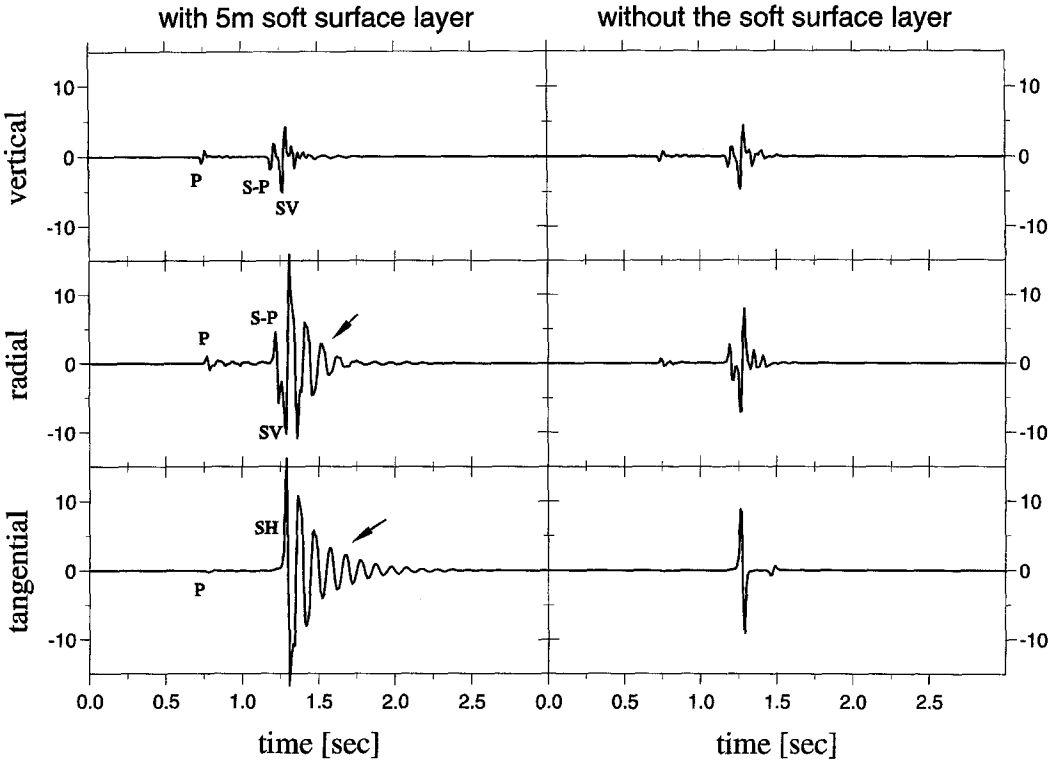

Figure 4. Synthetic seismograms for the Killari model (Table 2) with the 5-m soft-soil layer on the surface (*left*), compared with the reference seismograms (*right*) computed for the simplified model without the soil layer. A 45° dip-slip source at depth of 3 km is used in all cases, recorded at an epicentral distance of 3 km and an azimuth of 45°. The source wavelet used is proportional to $1/\tau \sin^3(\pi t/\tau)$, for $0 \leq t \leq \tau$, else 0 (equivalent to the first derivative of the moment function suggested by Brüstle and Müller, 1983), with $\tau = 50$ msec. Note the significant resonance effect in the two horizontal components (arrows) due to the soft surface layer. The small *P* phase in the tangential component is caused by the near-field effect.

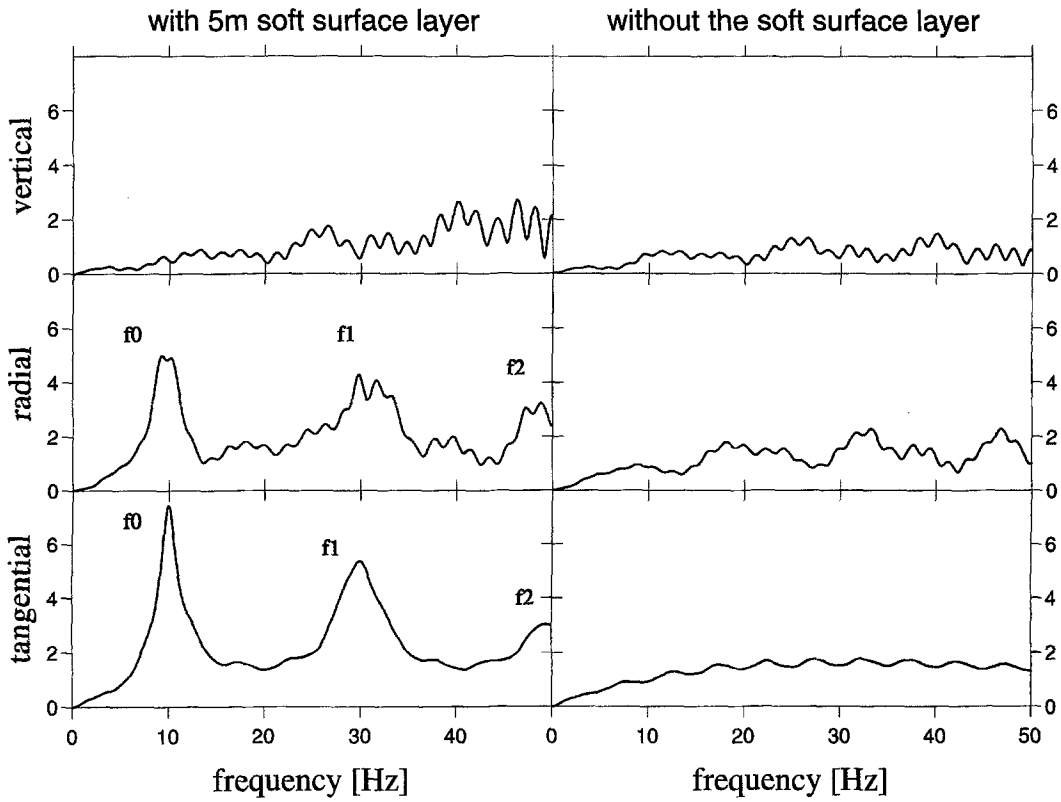

Figure 5. Amplitude spectra of the synthetic seismograms as shown in Figure 4, but for an impulse source ($\tau \rightarrow 0$). For the model with the 5-m soft surface layer, the two horizontal components are amplified by up to eight times at the fundamental resonance frequency of 10 Hz.

resonance band, dangerous seismic consequences would be expected. The soft surface layer over which many small farmhouses are built amplified significantly the ground motion and is partly responsible for the dramatical damage caused by the Latur earthquake. Synthetic seismograms should supply an accurate estimation of both the resonance frequency and the amplification factor. Figure 2 shows an example of typical aftershock seismograms recorded at the Killari station near the epicenter of the mainshock. It can be seen that the signals are significantly amplified at several high frequencies.

For synthetic seismograms, the simple but realistic model (Table 2) of Baumbach *et al.* (1994) has been used. In this model, a basaltic layer of 300 m is covered by a low-velocity soil layer of 5 m that might be responsible for the local amplification effects. A 45° dip-slip point source is placed at a depth of 3 km in the granitic half-space.

Figure 3 shows an example for normalized component of the surface displacement in the frequency-wavenumber domain. At high frequencies, the numerical problem with the original Thomson–Haskell propagator algorithm is quite significant. The cause is the thin soil layer with low velocities and high absorption. The problem is solved satisfactorily by using the orthonormalization technique.

Synthetic seismograms are computed for the Killari model at an epicentral distance of 3 km (Fig. 4). To estimate the site effect, the reference seismograms are computed for the simplified Killari model in which the 5-m soft soil on the surface is replaced by the same basalt underneath. From the comparison, we can see that the two horizontal components are clearly amplified by the soft soil, and in particular, the *S*-wave multiples cause nearly harmonic oscillations in the coda part. Figure 5 shows the amplitude spectra of the synthetic seismograms. The two horizontal components at the soft site are amplified by up to eight times at the resonance frequencies, while the site effect in the vertical component is much less significant.

Because of the large contrast to the basalt, the shear waves in the soil layer propagate almost vertically. The phase delay of the first multiple is then given by

$$\Delta = 2\pi \frac{2h}{V_s/f} - \pi, \tag{27}$$

where h is the soil thickness, V_s/f is the wavelength, and $-\pi$ represents the phase shift of a half wavelength due to reflection at the soil–basalt interface. Resonances will occur

when

$$\Delta = 2n\pi, \tag{28}$$

or

$$f_n = (2n + 1)\frac{V_s}{4h} \quad (n = 0, 1, \ldots). \tag{29}$$

For $V_s = 200$ m/sec and $h = 5$ m, the fundamental mode ($n = 0$) and the first overtone ($n = 1$) occur at 10 and 30 Hz, respectively.

Conclusions

A stable and efficient propagator algorithm with a global solution strategy for computation of Green's functions of a stratified half-space has been presented. The numerical difficulty of the original Thomson–Haskell propagator algorithm is fully avoided by a simple numerical procedure that makes the fundamental displacement vector in situ orthonormal. The new technique can be used to extend the matrix method as well as the numerical integration for general use. In the two test examples, the new algorithm has been applied to computation of static deformation due to a dislocation source and to synthetic seismograms. The results of the latter example have been used for modeling the high-frequency site effects observed in many aftershocks of the Latur earthquake, 1993, India.

Acknowledgments

This research has been supported by GeoForschungsZentrum Potsdam, Germany. We thank our colleagues M. Baumbach, H. Grosser, and R. Kind for their interest in this work and helpful discussions. B. L. N. Kennett is thanked for his review and helpful suggestions for the revision. S. M. Day pointed some misprints in the original manuscript.

References

Aki, K. and P. G. Richards (1980). *Quantitative Seismology—Theory and Methods,* Vols. I and II, Freeman and Co., San Francisco.

Baumbach, M., H. Grosser, H. G. Schmidt, A. Paulat, A. Rietbrock, C. V. Ramakrishna Rao, P. Solomon Raju, D. Starkar, and Indra Mohan (1994). Study of the foreshocks and aftershocks of the intraplate Latur earthquake of September 30, 1993, India, in *Latur Earthquake,* H. K. Gupta (Editor), Memoir of the Geological Society of India 35, 33–63.

Brüstle, W. and G. Müller (1983). Moment and duration of shallow earthquakes from Love-wave modeling for regional distances, *Phys. Earth Planet. Interiors* **32,** 312–324.

Chin, R. C. Y., G. W. Hedstrom, and L. Thigpen (1984). Matrix methods in synthetic seismograms, *Geophys. J. R. Astr. Soc.* **77,** 483–502.

Dunkin, J. W. (1965). Computation of modal solutions in layered, elastic media at high frequencies, *Bull. Seism. Soc. Am.* **55,** 335–358.

Fuchs, K. (1968). The reflection of spherical waves from transition zones with arbitrary depth-dependent elastic moduli and density, *J. Phys. Earth* **16** (special issue), 27–41.

Fuchs, K. and G. Müller (1971). Computation of synthetic seismograms with the reflectivity method and comparison with observations, *Geophys. J. R. Astr. Soc.* **23,** 417–433.

Gilbert, F. and G. E. Backus (1966). Propagator matrices in elastic wave and vibration problems, *Geophysics* **31,** 326–332.

Han, D. and J. Wahr (1995). The viscoelastic relaxation of a realistically stratified earth, and a further analysis of postglacial rebound, *Geophys. J. Int.* **120,** 287–311.

Haskell, N. A. (1953). The dispersion of surface waves on multilayered media, *Bull. Seism. Soc. Am.* **43,** 17–34.

Jovanovich, D. B., M. I. Husseini, and M. A. Chinnery (1974). Elastic dislocations in a layered half-space—I. Basic theory and numerical methods, *Geophys. J. R. Astr. Soc.* **39,** 205–217.

Kennett, B. L. N. (1983). *Seismic Wave Propagation in Stratified Media,* Cambridge University Press, Cambridge.

Kennett, B. L. N. and E. R. Engdahl (1991). Traveltimes for global earthquake location and phase identification, *Geophys. J. Int.* **105,** 429–465.

Kennett, B. L. N. and N. J. Kerry (1979). Seismic waves in a stratified half space, *Geophys. J. R. Astr. Soc.* **57,** 557–583.

Kind, R. (1983). Improvements to layer matrix method, *J. Geophys.* **53,** 127–130.

Knopoff, L. (1964). A matrix method for elastic wave problems, *Bull. Seism. Soc. Am.* **54,** 431–438.

Mindlin, R. D. (1936). Force at a point in the interior of a semi-infinity solid, *Physics* **13,** 195–202.

Mindlin, R. D. and D. H. Cheng (1950). Nuclei of strain in the semi-infinite solid, *J. Appl. Phys.* **21,** 926–930.

Okada, Y. (1992). Internal deformation due to shear and tensile faults in a half-space, *Bull. Seism. Soc. Am.* **82,** 1018–1040.

Schmidt, H. and G. Tango (1986). Efficient global matrix approach to the computation of synthetic seismograms, *Geophys. J. R. Astr. Soc.* **84,** 331–359.

Schwab, F., K. Nakanishi, M. Cuscito, G. F. Panza, G. Liang, and J. Frez (1984). Surface-wave computations and the synthesis of theoretical seismograms at high frequencies, *Bull. Seism. Soc. Am.* **74,** 1555–1578.

Takeuchi, H. and M. Saito (1972). Seismic surface waves, in *Methods in Computational Physics,* B. A. Bolt (Editor), Vol. 11, Academic, New York.

Thomson, W. T. (1950). Transmission of elastic waves through a stratified solid medium, *J. Appl. Phys.* **21,** 89–93.

Wu, P. and W. R. Peltier (1982). Viscous gravitational relaxation, *Geophys. J. R. Astr. Soc.* **70,** 435–485.

Xie, X.-B. and Z.-X. Yao (1989). A generalized reflection-transmission coefficient matrix method to calculate static displacement field of a stratified half-space by dislocation source, *Acta Geophys. Sinica* **32,** 270–280.

GeoForschungsZentrum Potsdam
Telegrafenberg
D-14473 Potsdam, Germany

Manuscript received 28 July 1998.